Application of aluminum diffusion coatings to mitigate the KCl-induced high-temperature corrosion

Kiamehr, Saeed; Lomholt, T. N.; Dahl, Kristian Vinter; Christiansen, Thomas Lundin; Somers, Marcel A. J.

Published in:
Materials and Corrosion

Link to article, DOI:
10.1002/maco.201609047

Publication date:
2017

Document Version
Publisher's PDF, also known as Version of record

Application of aluminum diffusion coatings to mitigate the KCl-induced high-temperature corrosion

S. Kiamehr*, T. N. Lomholt, K. V. Dahl, T. L. Christiansen and M. A. J. Somers

Pack cementation was used to produce $Fe_{1-x}Al$ and Fe_2Al_5 diffusion coatings on ferritic-martensitic steel P91 and a Ni_2Al_3 diffusion coating on pure nickel. The performance of diffusion coatings against high-temperature corrosion induced by potassium chloride (KCl) was evaluated by exposing the samples at 600 °C for 168 h in static lab air under KCl deposit. In addition, a salt-free experiment was performed for comparison. Microstructure, chemical and phase composition of the samples were analyzed with scanning electron microscopy (SEM), energy dispersive X-ray spectroscopy (EDS) and X-ray diffractometry (XRD) before and after the exposures. It was found that all the diffusion coatings formed protective oxides under salt-free exposure in air. Under the salt deposit, $Fe_{1-x}Al$ showed local failure while on large parts of the sample a protective layer had formed. Fe_2Al_5 was attacked over the entire surface and the dominant mode of attack was selective aluminum removal. Ni_2Al_3 showed excellent performance and no sign of attack was observed anywhere on the sample.

1 Introduction

Currently, there is a strong interest to substitute fossil fuels by potentially CO_2-neutral fuels. Biomass is an attractive option for electricity and heat generating power plants, especially in countries with large forest and agricultural resources. However, deposits formed during biomass combustion have shown to be so corrosive that the effective utilization of biomass has been hampered. During biomass firing, deposits rich in potassium chloride (KCl) develop on the heat exchangers and cause disastrous damage to the hot sections of the power plant, especially the superheater tubes. In order to keep the material loss at an acceptable level under these corrosive conditions, the temperature of the outlet steam is currently kept below 540 °C [1], thereby achieving a lower efficiency than with fossil fuels in a power plant of the same type. Accordingly, selection or development of materials with lower corrosion rates would allow a higher fire-side temperature and thus a higher steam temperature, so that effective utilization of biomass is realized in the future.

S. Kiamehr, K. V. Dahl, T. L. Christiansen, M. A. J. Somers
Department of Mechanical Engineering, Technical University of Denmark (DTU), Produktionstorvet, Building 425, Kongens Lyngby 2800 (Denmark)
E-mail: sabag@mek.dtu.dk

T. N. Lomholt
FORCE Technology, Park Alle 345, Brøndby 2605 (Denmark)

Unfortunately, field tests involving a wide range of commercial chromia-forming high-temperature alloys have not shown any promising results [2–6]. Therefore, the application of coatings relying on alumina (and/or silica) for corrosion protection has attracted attention. Among the different possibilities for alumina-forming materials, iron and nickel aluminides are interesting due to their high aluminum content.

Literature reports both satisfactory and poor achievements for aluminides depending on the combination of composition and exposure environment. *Li* et al. [7] evaluated the performance of bulk $Fe_{1-x}Al$ and NiAl in static lab air under KCl deposit at 650 °C. They reported excellent performance for NiAl while $Fe_{1-x}Al$ suffered from local attack in the form of selective aluminum removal. A similar trend was observed when the above-mentioned alloys were tested at 670 °C in static lab air under a molten KCl–NaCl mixture [8]. *Vokal* et al. [9] aluminized several alloys and studied their performance in static lab air under a KCl-50 mol%K_2SO_4 deposit at 650 °C. The studied alloys were ferritic–martensitic steel P91, austenitic stainless steels 17Cr-13Ni and Alloy 800 as well as nickel-base alloy Inconel 617. It was reported that all of the coatings were attacked. However, the extent of corrosion on Fe_2Al_5 coating formed on P91 was least pronounced as compared to the other investigated substrate/coating combinations. *Pan* et al. [10] investigated the behavior of Fe-21Ni-10Al and Fe-21.5Ni-10Al-12.5Cr (wt%) alloys against solid and vapor KCl at 650 °C in static lab air. They reported that none of these multiphase alloys, containing FeAl and NiAl phases, showed passive behavior.

Due to the similarity between the corrosion induced by KCl and NaCl [11,12] it is also relevant to mention a few literature reports addressing the performance of iron and nickel aluminides against NaCl. *McKee* et al. [13] exposed NiAl at 750 °C under a Na_2SO_4-10 wt%NaCl deposit with $N_2(g) + 76\%O_2(g) + 0.1\%SO_2(g)$ as the gas atmosphere. They observed catastrophic attack, which was attributed to chlorine evolved due to the sulfation of NaCl. *Smeggil* et al. [14] exposed NiAl to air contaminated with NaCl vapor at 900 °C and observed isothermal spallation of the oxide layer as well as growth of alumina whiskers. They attributed the whisker formation to a gas phase transport process induced by the presence of NaCl(g). *Magdziarz* et al. [15] investigated the corrosion of Ni_3Al under air and $NaCl–Na_2SO_4$ mixtures with different chloride to sulphate ratios. They reported an excellent performance for Ni_3Al up to 1000 °C for pure NaCl salt. Apart from this, also the performance of nickel and iron aluminides in oxygen and chlorine gas mixtures has been investigated in several studies [16–24]. In general, it has been observed in these investigations that the performance of aluminide coatings is superior to that of the corresponding chromia-forming substrate alloy.

The current investigation evaluates the performance of $Fe_{1-x}Al$, Fe_2Al_5 and Ni_2Al_3 diffusion coatings against KCl-induced high-temperature corrosion. Pack cementation was used to produce the coatings. In the present process variant, the substrate alloy is embedded in a powder pack consisting of the aluminum metal source, alumina as an inactive filler material and aluminum chloride as an activator. Heating the mixture to a sufficiently high temperature in an inert atmosphere of argon, to prevent oxide formation, initiates the process by chloride-based surface activation and the formation of volatile aluminum chlorides. These chlorides decompose at the activated sample surface leaving behind an aluminum deposit. Reactive interdiffusion between the deposited aluminum and the components in the substrate leads to the formation of intermetallic aluminides [25,26].

2 Experimental procedure

Pure nickel (99.99 wt%) and ferritic–martensitic steel P91 (Fe-9Cr-1Mo-0.5Si-0.2 V wt%) were chosen as the substrate materials. Samples were coupons of $\sim 20 \times 8 \times 0.3$ mm cut with a precision cutter. Prior to pack aluminizing, the samples were ground with 500 grit SiC paper and subsequently cleaned with ethanol. Pack cementation was done in a tube furnace in argon atmosphere with a flowrate of 100 ml/min. The pack powder consisted of aluminum, anhydrous aluminum chloride as the activator and alumina powder as inert filler in the amounts shown in Table 1. For synthesis of a $Fe_{1-x}Al$ diffusion coating, the aluminum activity in the pack was adjusted by adding iron powder to the pack mixture. Powders for the pack were weighed and mixed thoroughly. Powder and samples were then packed into alumina containers that were inserted into the tube furnace. The pack was heated to 650 °C using a heating rate of ~10 °C/min, held for the process time listed in Table 1 and subsequently cooled to room temperature inside the furnace in the argon flow.

Table 1. Parameters of the pack cementation process

	Pack content (wt%)				
Phase to be formed	Al	Fe	$AlCl_3$	Al_2O_3	Duration (h)
$Fe_{1-x}Al$	10	10	6	74	20
Fe_2Al_5	10	–	6	84	6
Ni_2Al_3	10	–	6	84	8

After processing, the samples were separated from the pack and cleaned in an ultrasonic bath of ethanol. Subsequently one sample of each aluminide phase was covered for 2/3 of its length with a ~1 mm thick layer of KCl powder (particle size 63–90 μm) and was exposed for 168 h at 600 °C in static lab air. In addition, for all the diffusion coatings a salt-free exposure was performed for comparison. The as-coated and exposed samples were investigated with XRD to determine their phase composition. For this purpose, a Bruker D8 Discover X-ray diffractometer was used and the analysis for each sample was performed under both grazing-incidence and Bragg–Brentano configurations. CrK_α ($\lambda = 2.2897$ Å) radiation was used as the incident beam. Thereafter, cross sections of the samples were prepared by embedding them in epoxy resin and grinding/polishing, using ethanol as lubricant. The microstructure of the samples was studied using an Inspect S SEM equipped with an EDS detector. Imaging was performed in back-scattered electron (BSE) mode.

3 Results

3.1 Performance of $Fe_{1-x}Al$ on P91

The microstructure of the aluminized surface is given in Fig. 1a. The diffusion layer appeared uniform in thickness (~5–7 μm) but at a few locations no layer had formed. No cracks were detected in the diffusion layer. In addition, voids were occasionally observed in the diffusion layer (marked with white arrows in Fig. 1a). Formation of voids during pack cementation has previously been attributed to the Kirkendall effect [27–29]. Another microstructural feature is the presence of particles, appearing as needles, in the lower part of the layer (marked with black arrows in Fig. 1a). Nitrogen was detected with EDS spot analysis on the needles. This has been attributed to the formation of aluminum nitride (AlN) by *Metsäjoki* et al. [29]. The microstructure after the salt-free exposure is given in Fig. 1b. Clearly, exposure in static lab air without the salt did not lead to a significant surface degradation. Concentration profiles of aluminum and chromium, acquired with EDS line analysis before and after the oxidation, are given in Fig. 1c and demonstrate that continued interdiffusion of components from the coating and from the substrate alloy has occurred. The effect of prolonged interdiffusion during oxidation is clearly observed for the aluminum concentration profile: the maximum concentration at the surface is reduced and the penetration into the substrate has increased.

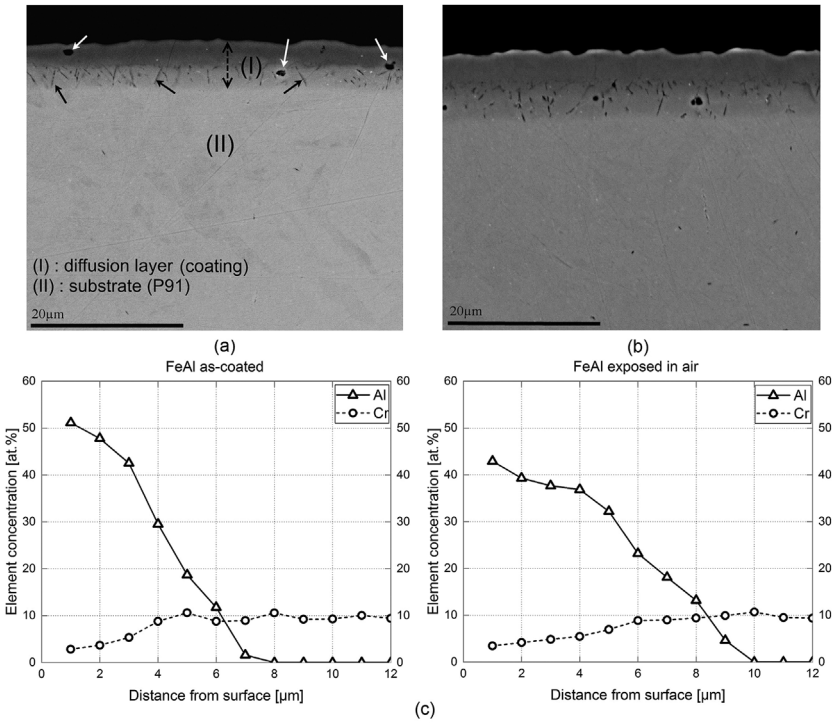

Figure 1. Microstructure of the $Fe_{1-x}Al$ coating on P91: (a) as-coated, (b) air-oxidized for 168 h at 600 °C without KCl, (c) concentration profiles of aluminum and chromium in the as-coated and air-oxidized (without salt) samples

The sample subjected to oxidation under a KCl deposit was virtually unaffected on large areas of the surface (Fig. 2a). However, on both the salt-free part of the sample (Fig. 2b) and on the salt-covered part (Fig. 2d) local attack could be found. At a few locations, both the coating and the underlying alloy were corroded (Fig. 2d). Results of EDS spot analysis (Fig. 2b) show that in a region where the local attack on the coating had taken place, a significant dilution in aluminum could be found while an aluminum-rich corrosion product has formed (Fig. 2c).

Figure 3 shows the distribution of the alloying elements in the corrosion product morphology at a location where no significant attack has taken place. A thin corrosion product is observed on the coating and potassium (without chlorine) appears enriched all over the surface, suggesting the development of a potassium containing compound.

Figure 4 shows the distribution of the elements throughout the corrosion product at a location where the local attack has affected both the coating and the underlying alloy. The outer oxide is rich in iron and contains small amounts of aluminum. The inner oxide is rich in chromium and contains remnants of the aluminum close to the original coating's surface. Nitrogen enrichment can be observed close to the region where local attack had occurred. EDS spot analysis also reveals the presence of small amounts of potassium (up to 4 at%) and chlorine (up to 3 at%) in the corrosion products that have developed in the alloy. As follows from the difference in intensity in the chlorine map, the outward growing corrosion product is free of chlorine, because the gray level in the surrounding epoxy is higher. Some potassium appears to be present in the outward growing corrosion product as well.

Figure 5 shows X-ray diffractograms for the samples before and after the exposures. The diffractograms confirm that the as-coated layer consists of $Fe_{1-x}Al$ in the bulk with a minor amount of (possibly) Fe_2Al_5 at the surface. The diffractogram for the sample subjected to the salt-free exposure does not show clear peaks of any oxide, but hints of the presence of Fe_2O_3 are found at 50 and 54° 2θ. After exposure to KCl clearly two peaks around 50 and 54° 2θ can be detected, which can be attributed to Fe_2O_3. In addition, the peak around 40° 2θ as well as a faint background elevation around 82° 2θ indicate the presence of Fe_3Al. No potassium containing compound could be identified. Compared to the as-coated microstructure, the peaks were slightly shifted to higher 2θ angles after both exposures.

3.2 Performance of Fe_2Al_5 on P91

The microstructure of the as-produced coating is given in Fig. 6a. The deposited Fe_2Al_5 often showed cracks in the growth direction indicating the release of tensile stresses in the coating. The diffusion layer has a non-uniform thickness (~20–55 μm) and contains several phases. In contrast to the observations for $Fe_{1-x}Al$, neither voids nor needle-looking features can be observed in the as-deposited layer. EDS mapping shows that a chromium-rich phase, appearing as stringers of particles, is present in the microstructure and in principle extends from the alloy-coating interface to the surface, albeit more concentrated close to the substrate. In addition, chromium and silicon-rich particles are present in the outer part of the coating (Fig. 6b).

Salt-free exposure did not lead to significant surface degradation. Continued interdiffusion between Fe_2Al_5 and the

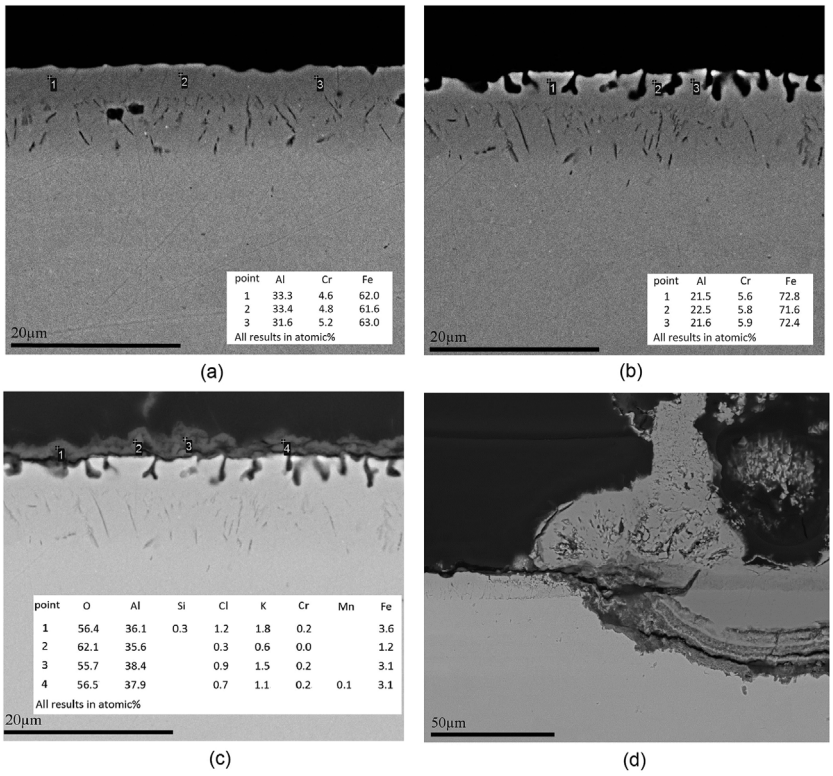

Figure 2. $Fe_{1-x}Al$ coating on P91 after corrosion of the partly KCl-covered sample exposed for 168 h in air: (a) a location without significant degradation, (b) local attack on salt-free part of the sample, (c) the same area as in *b* but with higher brightness and lower contrast to reveal the corrosion product, (d) local attack on the KCl-covered part affecting both the coating and the alloy. Note that the chlorine in the EDS results can be partly from the epoxy used for embedding the sample (Fig. 3)

substrate alloy occurred during the exposure (Fig. 7a): voids and nitrogen-containing needle-like features have developed (marked by solid and dashed black arrows, respectively in Fig. 7a). Moreover, close to the surface aluminum-diluted regions appearing as "islands" were sparsely observed (marked by white arrows in Fig. 7a). EDS spot analysis in such islands gave values between 54 and 59 at% Al. An EDS line scan across the coating is given in Fig. 7b: the aluminum profile (after the

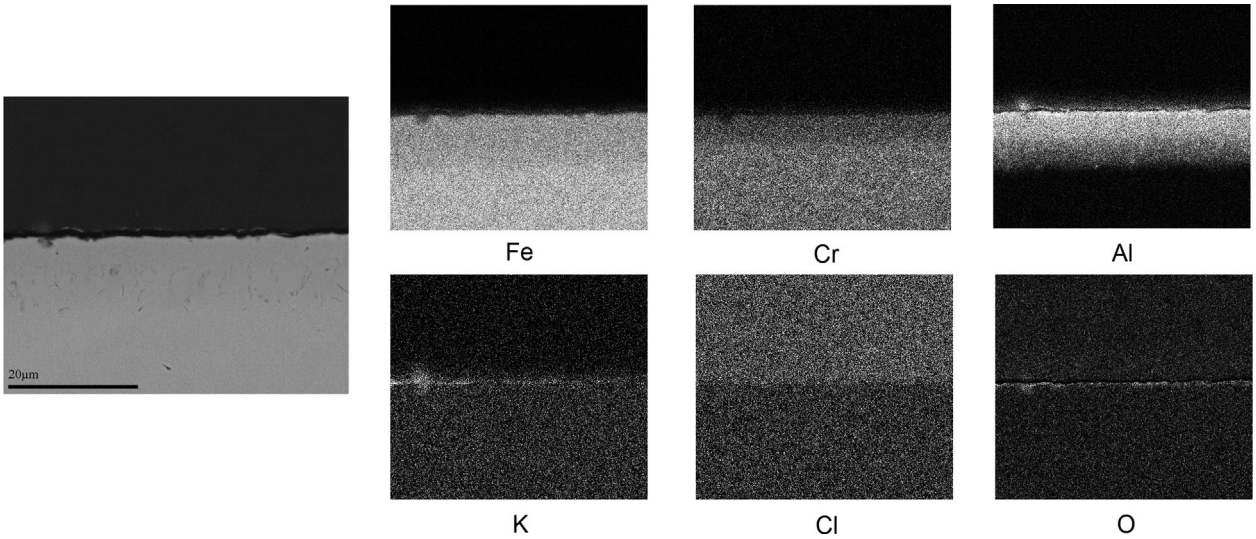

Figure 3. Distribution of the elements throughout the corrosion product on $Fe_{1-x}Al$-coated P91 exposed under air + KCl(s) at 600 °C for 168 h at a location where no significant attack has taken place. Note that the chlorine on the upper half of its map comes from the epoxy used for embedding the sample

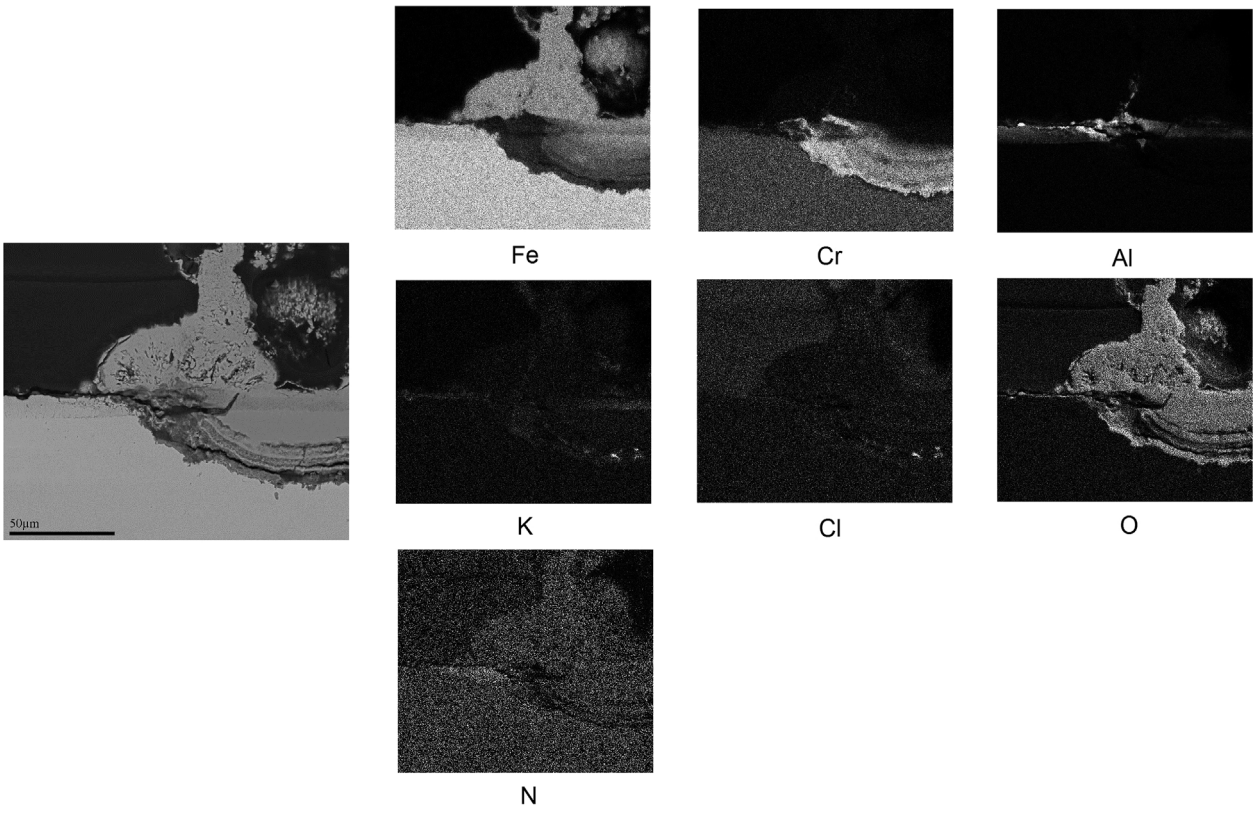

Figure 4. Distribution of the elements throughout the corrosion product on $Fe_{1-x}Al$-coated P91 exposed under air + KCl(s) at 600 °C for 168 h at a location where the local attack has affected both the coating and the underlying alloy. Note that the chlorine on the upper half of its map comes from the epoxy used for embedding the sample

salt-free exposure) showed a small step at about 50 at% which coincides with the position of the interface between Fe_2Al_5 and the interdiffusion zone. It should be noted that for this coating the shift of aluminum concentration profile to a shallower depth after the exposure (Fig. 7b) is not necessarily a consequence of aluminum consumption by interdiffusion, but is, at least partly, caused by the non-uniform thickness of the as-grown layer.

In contrast with the passive behavior observed for the salt-free exposure, the presence of KCl caused severe attack on Fe_2Al_5, even on the salt-free part. Generally, selective removal of aluminum and formation of a voluminous and porous aluminum-rich corrosion product on top of the coating was observed (Fig. 8a). EDS spot analysis on the aluminum-diluted areas close to the surface gave an average value of 51 at% aluminum and 6 at% chromium. Dilution of aluminum in

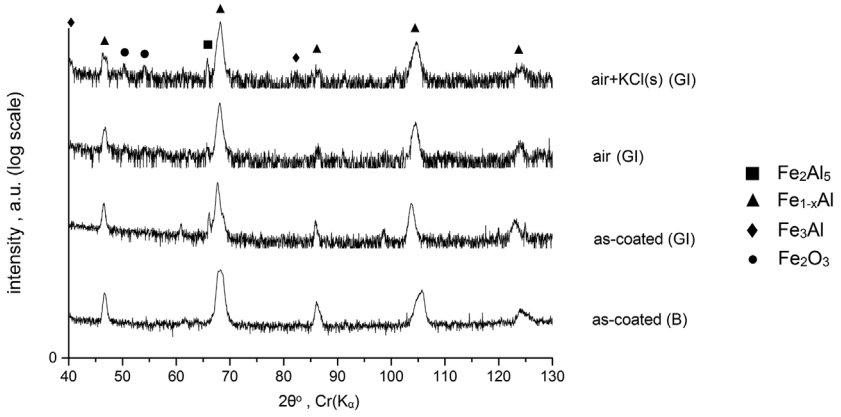

Figure 5. Phase composition of the $Fe_{1-x}Al$-coated P91 before and after the exposures. B denotes measurement in Bragg–Brentano configuration. The rest of the measurements have been performed in grazing-incidence (GI) configuration at an incidence angle of 2 ° to enhance the surface sensitivity

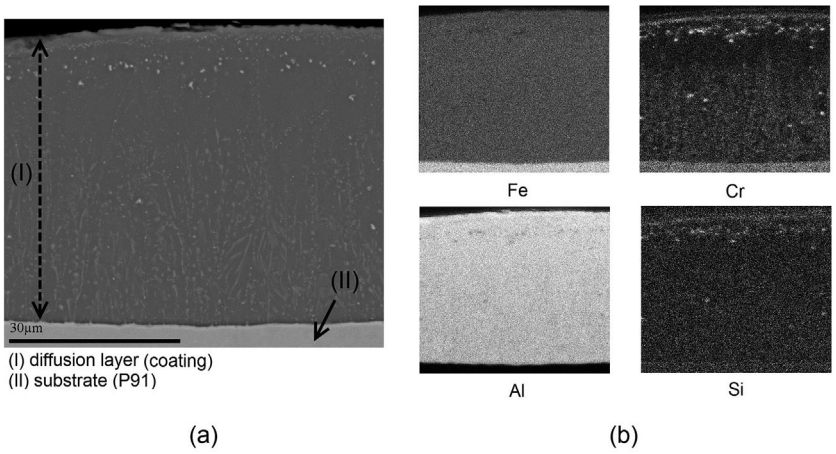

Figure 6. (a) As-coated Fe_2Al_5 on P91. A crack-free location is shown in this micrograph. (b) Distribution of iron, aluminum, chromium, and silicon throughout the coating (shown in *a*) suggesting the formation of a chromium-rich phase as well as a chromium-silicon-rich phase in the coating

these areas was coupled to enrichment in iron and chromium. An example of this mode of attack is shown in Fig. 8a with further details shown in Fig. 8c. In a few cases, Fe_2Al_5 was completely consumed and a thick double layer oxide, in addition to the outermost highly porous oxide, had formed (Fig. 8b). In both cases potassium was found throughout the corrosion product. EDS spot analysis on the porous aluminum-rich outer oxide gave potassium contents up to 10 at%. Distribution of the main metallic elements as well as potassium and oxygen over the above-mentioned corrosion product morphologies are given in Figs. 9 and 10, respectively. In the first corrosion morphology, only aluminum, among the major elements that constitute the coating, is associated with oxygen (Fig. 9). In the second corrosion morphology, all the major coating elements are associated with oxygen i.e. corroded (Fig. 10).

Figure 11 shows the results of phase analysis with XRD. The as-coated layer consists of Fe_2Al_5 with a small amount of Cr_3Si consistent with the mapping in Fig. 6b and aluminum concentration profile in Fig. 7b. The salt-free exposure did not

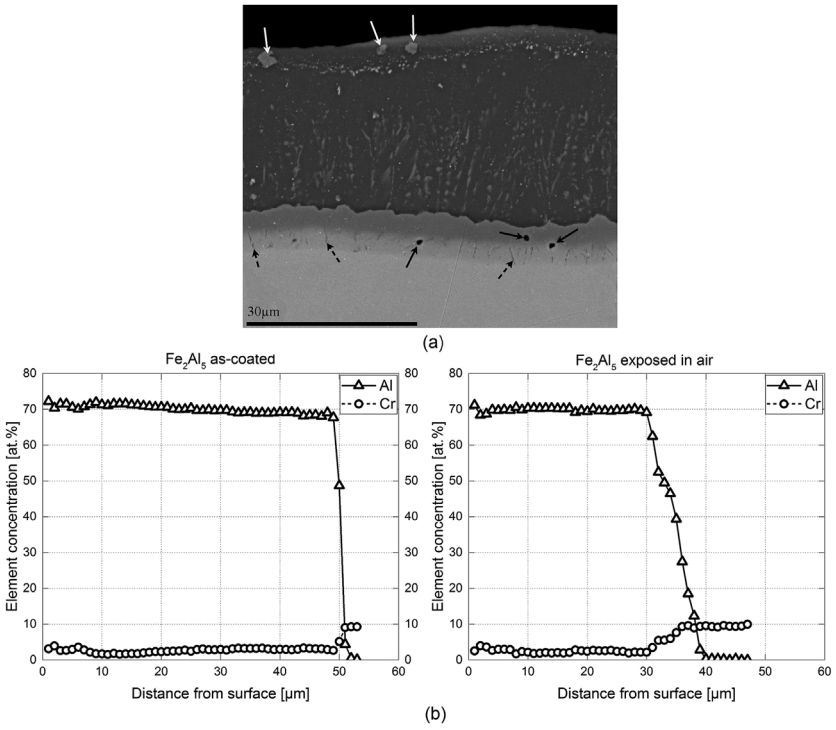

Figure 7. (a) Microstructure of the alloy and the coating after the salt-free exposure. (b) Aluminum and chromium concentration profiles before and after the salt-free exposure

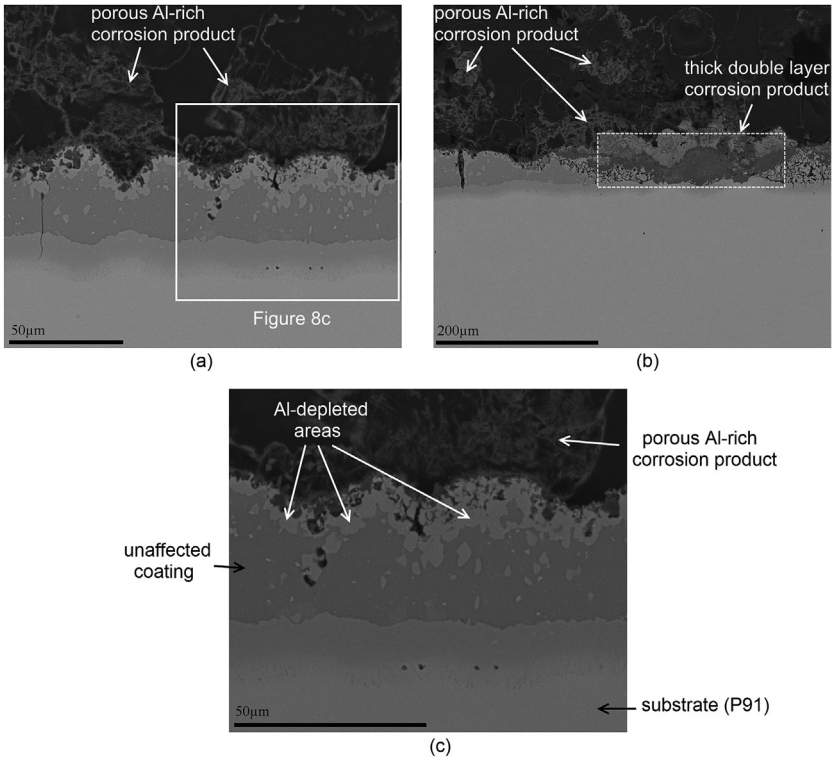

Figure 8. (a and b) Corrosion product morphologies observed for Fe_2Al_5 coating on P91 exposed under air + KCl(s) at 600 °C for 168 h. (c) Magnification of the boxed area in *a* showing the aluminum-depleted areas and unaffected coating

lead to a significant change in phase composition as compared to the as-deposited coating. Only a slight background elevation could be detected around 52° 2θ. The diffractogram after the exposure to KCl suggests the presence of α-Al_2O_3. However, no other oxide and/or potassium containing compound could be identified. In addition, increasing the incidence angle to 5° (not shown in Fig. 11) revealed that a small amount of $Fe_{1-x}Al$ had formed as well, which would be consistent with aluminum dilution due to the corrosion.

3.3 Performance of Ni_2Al_3 on Ni

Figure 12a and b show the microstructure of the diffusion coating on a Ni substrate before and after the salt-free exposure.

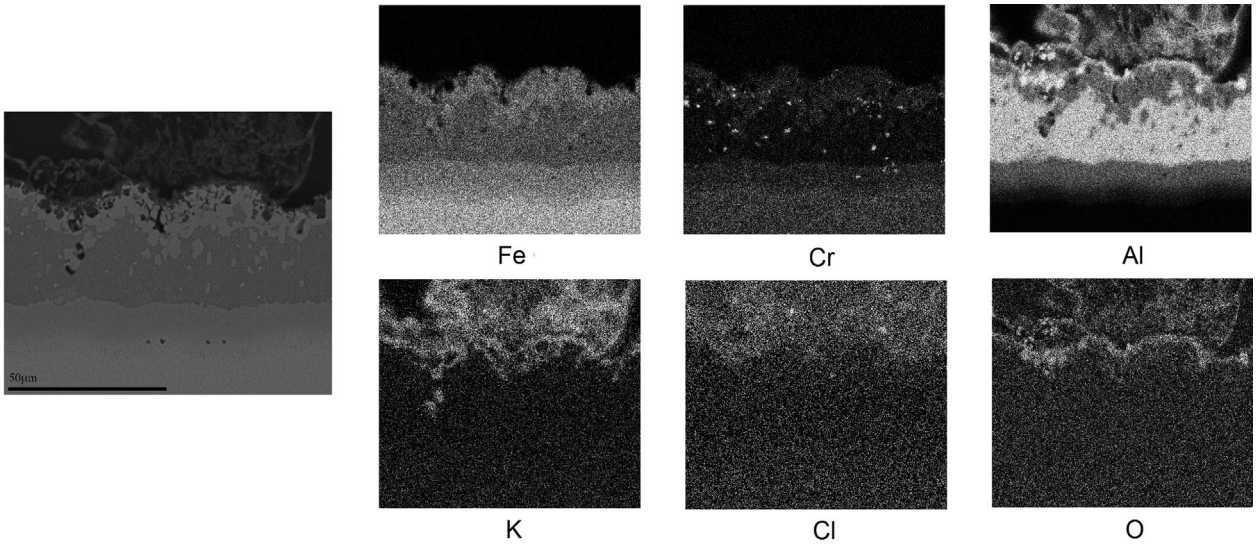

Figure 9. Distribution of the elements throughout the corrosion product on Fe_2Al_5-coated P91 exposed under air + KCl(s) at 600 °C for 168 h. The location shown in this figure is where the coating is partially corroded

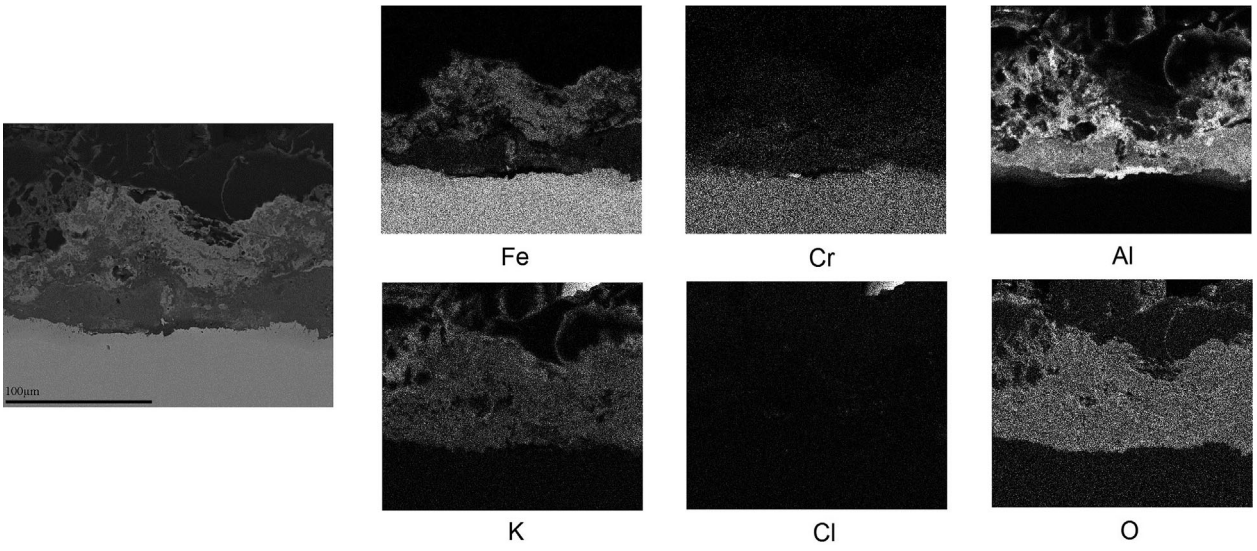

Figure 10. Distribution of the elements throughout the corrosion product on Fe_2Al_5-coated P91 exposed under air + KCl(s) at 600 °C for 168 h. The location shown in this figure is where the coating is completely corroded

The as-coated layer showed non-uniform thickness varying between 50 and 70 μm. No deep penetrating vertical cracks, as observed for Fe_2Al_5, were found. However, occasionally shallow-penetrating transgranular cracks could be observed close to the surface. The contrast differences in the BSE image (Fig. 12) shows the presence of a thin (<5 μm) layer of intermediate phases at the coating/substrate interface. The amount of such intermediate phases constitutes only a very small fraction of the entire coating. No evidence for high-temperature corrosion attack was found after the salt-free exposure. Continued interdiffusion between the diffusion coating and the nickel substrate led to the growth of intermediate phases (Fig. 12b). EDS line scans over the thickness of the coating are given in Fig. 12c. For the as-coated sample, the drop in aluminum content is abrupt while the aluminum concentration profile on the exposed sample is more diffuse. Again, similar to the case for Fe_2Al_5, the shift of the transition from diffusion coating to the substrate (Fig. 12c) is at least partly caused by the non-uniform thickness of the as-deposited coating and cannot be attributed entirely to interdiffusion.

The microstructure of the sample after exposure to KCl (Fig. 13a) was similar to that without the salt deposit, indicating that the coating is not attacked by the salt. No evidence for local attack could be observed anywhere on the sample. Analogous to the salt-free exposure interdiffusion took place between the nickel substrate and the coating, leading to the formation of new intermediate phases. EDS spot analysis (Fig. 13b) suggests the formation of $Ni_{1-x}Al$, Ni_5Al_3, and Ni_3Al intermetallic phases similar to the salt-free exposure. Mapping of the cross section gave a faint indication of a thin aluminum enriched corrosion product formed on the surface (Fig. 14).

Figure 15 shows the diffractograms corresponding to the samples before and after the exposures. After the salt-free exposure, in addition to the Ni_2Al_3 peaks, only minor peaks corresponding to $Ni_{1-x}Al$ could be detected. However, repeating the XRD in Bragg–Brentano condition did not reveal any $Ni_{1-x}Al$

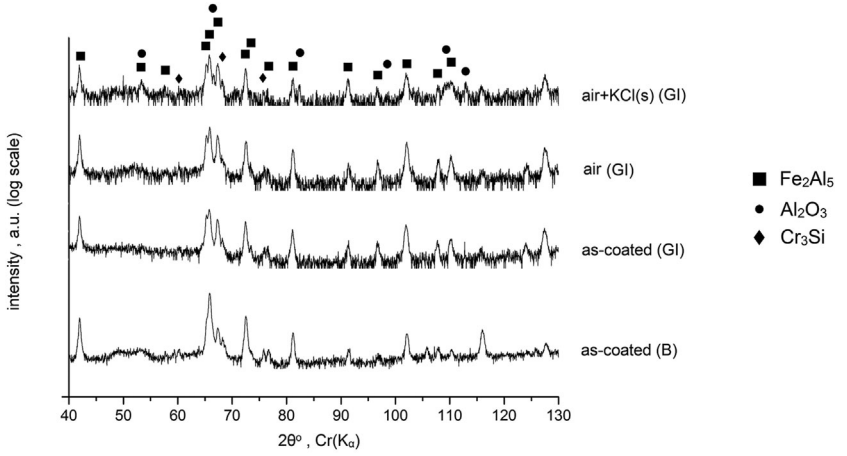

Figure 11. Phase composition of the Fe_2Al_5-coated P91 before and after the exposures. B denotes measurement in Bragg–Brentano configuration. The rest of the measurements were performed in grazing-incidence (GI) configuration at an angle of 2°

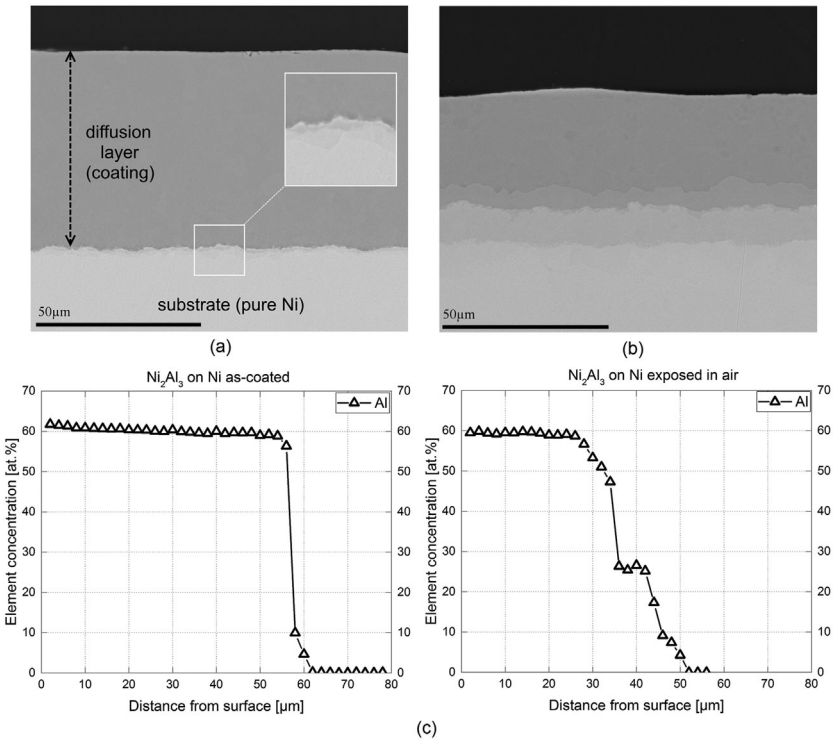

Figure 12. Microstructure of Ni_2Al_3 coating on Ni in (a) as-coated and (b) oxidized in salt-free condition (c) aluminum profile before and after the salt-free exposure

peaks (not shown in Fig. 15). The sample oxidized under KCl deposit did not show any peaks other than those of the as-coated sample.

4 Discussion

4.1 $Fe_{1-x}Al$ on P91

The observation with XRD that all the peaks in the diffractogram after the salt-free exposure (Fig. 5) match those for the diffractogram of the as-coated sample indicates that the oxide formed in the absence of KCl is too thin (or amorphous) to be detected with GI-XRD. In addition, there were no indications of the presence of a thick (i.e., fast-growing) oxide layer on the surface (Fig. 1b). This may confirm the presence of a very thin protective oxide layer. The shift in the XRD peaks of $Fe_{1-x}Al$ in Fig. 5 is consistent with a reduction of the aluminum content due to continued interdiffusion (Fig. 1c) and/or oxidation. Nevertheless, $Fe_{1-x}Al$ is still present after 168 h of exposure. A relatively broad homogeneity range of the $Fe_{1-x}Al$ phase suggests that diffusion of aluminum (and iron) in this phase is sufficiently fast to form and maintain a protective oxide layer in the salt-free exposure. Therefore, when an

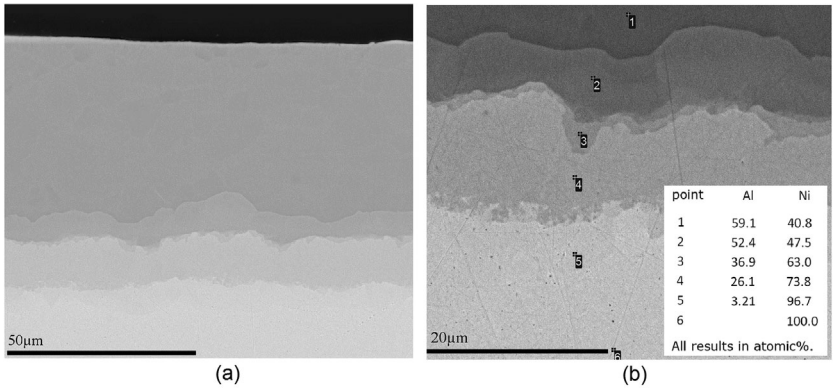

Figure 13. Microstructure of the Ni_2Al_3 coating on pure Ni exposed under air + KCl(s) at 600 °C for 168 h (a) entire coating and substrate (b) interface between the substrate and the coating showing the formation and/or growth of intermetallic phases due to continued interdiffusion

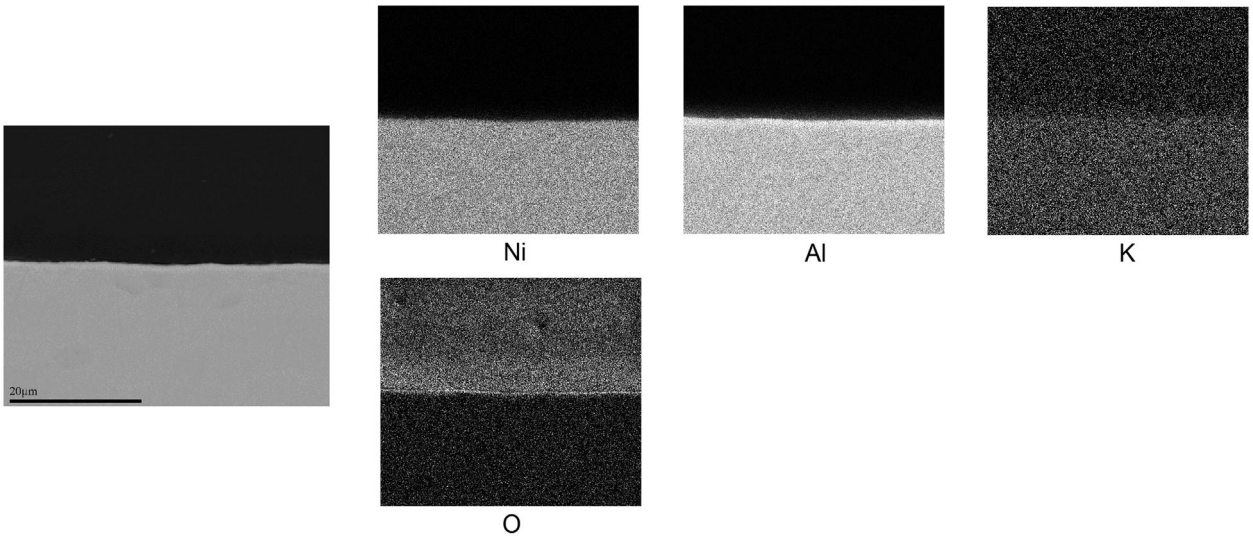

Figure 14. Distribution of the elements throughout the corrosion product on Ni_2Al_3-coated pure nickel exposed under air + KCl(s) at 600 °C for 168 h

aluminum potential gradient exists near the surface, due to the oxygen presence in the environment and higher affinity of aluminum to oxygen compared to that of iron, an aluminum-enriched oxide can be established rapidly and protect the alloy from further oxidation.

The local failure of the diffusion coating on P91 (Fig. 2d), after exposure to the oxidizing environment under KCl deposit is similar to the behavior of Fe-45 at%Al model alloy reported by *Li* and *Spiegel* [7]. In the current study, it was observed that such failure was associated with an enrichment of potassium (unaccompanied by chlorine) at the same locations as enrichments in aluminum and oxygen. This finding suggests that a reaction between the KCl and the aluminum in the oxide has been possible, which paves the way for further corrosion. FactSage [30] calculations yield, among other possibilities, that KAl_9O_{14} formation is the thermodynamically preferred result of a reaction between solid or gaseous KCl and Al_2O_3:

$$\mathrm{KCl(s)} + (9/2)\mathrm{Al_2O_3} + (1/4)\mathrm{O_2(g)} = \mathrm{KAl_9O_{14}(s)} + (1/2)\mathrm{Cl_2(g)};\ \Delta G^{\circ}(600^{\circ}\mathrm{C}) = +48.5\ \mathrm{KJ} \quad (1)$$

$$\mathrm{KCl(g)} + (9/2)\mathrm{Al_2O_3} + (1/4)\mathrm{O_2(g)} = \mathrm{KAl_9O_{14}(s)} + (1/2)\mathrm{Cl_2(g)};\ \Delta G^{\circ}(600^{\circ}\mathrm{C}) = -42.5\ \mathrm{KJ} \quad (2)$$

Reaction (1) has a positive ΔG°. However, it will partially progress as there is no chlorine in the inlet gas and therefore $P_{Cl2(g)}$ is below the equilibrium value for reaction (1). Reaction (2), considering gaseous KCl, is thermodynamically feasible and although the equilibrium vapor pressure of KCl(s) at 600 °C is only 4×10^{-6} atm [31] it will always progress. Accordingly, it is

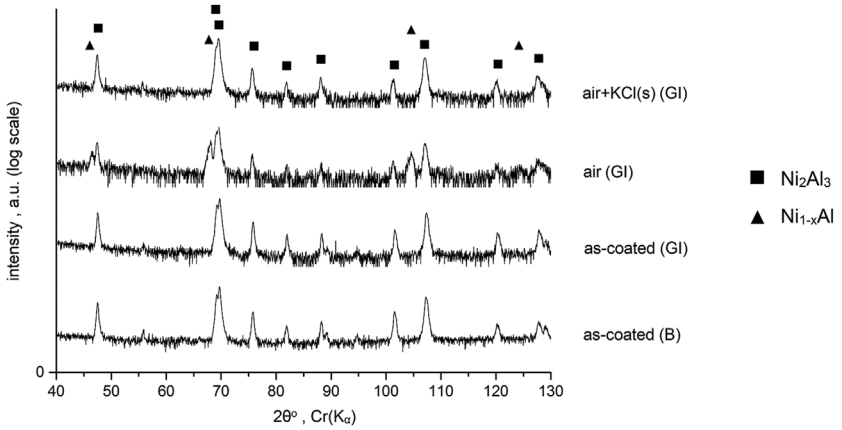

Figure 15. Phase composition of the Ni_2Al_3-coated pure nickel before and after the exposures. B denotes measurement in Bragg–Brentano configuration. The rest of the measurements have been performed in grazing-incidence (GI) configuration at an angle of 2°

not far from expectation that the thin Al_2O_3 formed on the coating will be damaged due to the presence of KCl. A reaction product between KCl and Al_2O_3 was not observed in a previous study [32] where the reactivity of KCl with α-Al_2O_3 powder was investigated with XRD. This can be attributed to several reasons: a difference in the Al_2O_3 polymorphs in the two studies or the inability of XRD to characterize amorphous and minor contents (less than 3 wt%). Moreover, *Folkesson* et al. [33] propose an electrochemical mechanism for the KCl-induced high-temperature corrosion which involves evolution of, among other species, potassium hydroxide (KOH). A reaction between KOH and Al_2O_3 is spontaneous and can account for the presence of K–Al–O compound(s).

Provided that the aluminum supply (concentration and diffusivity) after an initial attack is sufficient the alloy can re-passivate. This could apply for the case shown in Fig. 2a where the aluminum content is about 32 at% and $Fe_{1-x}Al$ is still stable. The presence of potassium without chlorine (mapping in Fig. 3) has another implication as well. It indicates that chlorine was released due to an interaction between the alloy and KCl. In the literature, it is reported that chlorine can cause selective removal of the more reactive alloying elements, like aluminum, by volatilization, i.e., the reverse of the deposition process [2,34–38]. Therefore, it is not surprising to detect significantly lower aluminum contents in the coating as compared to the salt-free exposure. Such aluminum depletion has also been observed on Fe-45 at%Al model alloy by *Li* et al. [7] and has been attributed to the presence of chlorine. In the current study, formation/deposition of a thick aluminum oxide on the surface of the alloy (as shown in Fig. 2c) and the low content of residual aluminum (21 at%) also suggests that chlorine is involved in de-aluminization of the coating. When the coating lacks sufficient aluminum to form a protective oxide a thick fast-growing oxide and internal nitrides (Fig. 4) will form. In summary, it appears that due to interdiffusion and the presence of KCl the aluminum content of the diffusion coating is reduced. It is anticipated that as long as the composition is within the stability range of $Fe_{1-x}Al$ (i.e., the original $Fe_{1-x}Al$ layer is sufficiently thick) the alloy can re-passivate and avoid significant material loss. Clearly, in the present experiment the $Fe_{1-x}Al$ diffusion coating is not thick enough all over the surface. Therefore, aluminum dilution of the diffusion coating will occur after a very short exposure time as compared to the expected lifetime of critical components in power plants.

4.2 Fe_2Al_5 on P91

For Fe_2Al_5 on P91 the diffractogram obtained after the salt-free exposure (Fig. 11) shows no oxide peaks and no change as compared to the diffractogram of the sample before the exposure. This suggests that an aluminum-rich protective oxide has formed that is too thin (or amorphous) to be detected with GI-XRD (Note that surface roughness can compromise quantitative analysis of X-ray diffractograms determined under grazing incidence conditions). The presence of a thin oxide layer would be consistent with the absence of an oxide layer in the SEM image (Fig. 7a). *Metsäjoki* et al. [29] reported the formation of γ-Al_2O_3 on Fe_2Al_5-coated P91 exposed at 650 °C for 1000 h in air.

If aluminum is removed to form aluminum oxide, less aluminum-rich intermetallic phases will form adjacent to the oxide. Since Fe_2Al_5 has a limited homogeneity range (e.g., as compared to $Fe_{1-x}Al$) the slightest aluminum removal leads to the formation of intermetallic phases with lower aluminum content. Results of EDS spot analysis on the islands close to the surface with an aluminum content 54–59 at% (indicated by white arrows in Fig 7a) would be reconcilable with $Fe_{1-x}Al$. The aluminum content higher than dissolvable in $Fe_{1-x}Al$ is explained from the large electron-sample interaction volume, which leads to an overestimation of the aluminum intensity from the surrounding Fe_2Al_5. The salt-free exposure also leads to continued interdiffusion between coating and alloy substrate. The presence of a step in the concentration profile near 50 at% aluminum, shown in Fig. 7b, is a consequence of the formation of $Fe_{1-x}Al$ underneath Fe_2Al_5. However, due to the wide homogeneity range in $Fe_{1-x}Al$ the step on the concentration profile is not flat. Similar to the case for the $Fe_{1-x}Al$ coating on P91, voids and needle-like features develop within the interdiffusion zone.

The presence of KCl during the exposure has a remarkable impact on Fe_2Al_5. Unlike $Fe_{1-x}Al$ which only showed local failure, the surface of Fe_2Al_5 was severely attacked. Figure 8a and the mapping in Fig. 9 show that, similar to the results by *Vokal* et al. [9], aluminum was selectively removed and iron/chromium were enriched. In addition, it turns out that the removed aluminum is present outside the original coating's surface matching the maps of oxygen and potassium. Absence of AlN just underneath the corrosion product (within the aluminum-diluted region in the coating) shows that the corrosion product is outward-growing.

Conformity of the aluminum map in Fig. 9 with that of oxygen is consistent with the α-Al_2O_3 peaks found in the diffractogram shown in Fig. 11. However, presence of a potassium-aluminum-oxygen compound could not be confirmed by XRD (Care must be taken interpreting grazing incidence diffractograms on rough surfaces). A small spike near 71° on the diffractogram could be attributed to several potassium-aluminum-oxygen compounds (e.g., $K_{1.6}Al_{11}O_{17}$, KAl_5O_8). However, all these phases have other peaks that cannot be retrieved in the diffractogram. Other possibilities for the absence of the sought compound(s) can be that it is formed in small amounts, it has an amorphous structure or it is obscured due to peak overlaps.

The microstructure in Fig. 8c shows that aluminum removal is not limited to the coating surface; aluminum-diluted areas are also found in the middle of the Fe_2Al_5 layer (in a two-dimensional image these regions appear as light-contrast "islands" in the middle of the coating in Fig. 8c). The depth of aluminum removal as well as the morphology of the corrosion product strongly suggests that the mechanism of dilution is the formation of volatile aluminum chloride (similar to Fig. 2c). It appears that if the aluminum-diluted area maintains a sufficient aluminum content (after an initial removal) it has the possibility to re-passivate. EDS spot analysis on several aluminum-diluted areas similar to Fig. 8a gave values around 51 at% for the residual aluminum content. This is consistent

with the detection of $Fe_{1-x}Al$ when the GI-XRD was performed at 5° and describes why the corrosion does not continue on some parts of the Fe_2Al_5. Description of the corrosion morphology shown in Fig. 8b is not as straight-forward as that in the Fig. 8a. However, one can speculate a case where the de-aluminization of Fe_2Al_5 is locally so severe that the residual aluminum content is insufficient to support formation of a protective oxide at a later stage. In such a case, the alloy cannot re-passivate after the initial stages of the attack (i.e., de-aluminization by volatilization) and eventually a double layer oxide rich in iron on top and aluminum at the bottom will form underneath the earlier corrosion products.

4.3 Ni_2Al_3 on Ni

The salt-free exposure of Ni_2Al_3 on Ni did not lead to a visible degradation of the surface. Again, lack of detection of oxide by GI-XRD indicates that it is very thin or amorphous. This is consistent with the micrograph shown in Fig. 12b that demonstrates oxidation resistant behavior. The only visible effect with SEM was the continued interdiffusion of aluminum from the coating and nickel from the substrate. This was evidenced by the thickening of the layer consisting of intermediate phases. The observation that $Ni_{1-x}Al$ had formed close to the surface of Ni_2Al_3 after the salt-free exposure requires further study as this was not observed for the KCl-affected sample.

In contrast with the observations for the $Fe_{1-x}Al$ and Fe_2Al_5 coatings the presence of KCl did not lead to a significant effect on Ni_2Al_3. The diffractogram of the salt-affected sample perfectly matched that of the as-coated sample and no fast-growing oxide was observed on the sample when the cross section was studied with SEM. Considering the interaction between KCl and $Fe_{1-x}Al$ or Fe_2Al_5 (e.g., mapping in Fig. 9) and the fact that the strongest oxide-forming element for all the coatings is aluminum, a similar interaction would be expected with Ni_2Al_3 and KCl. However, the mapping in Fig. 14 does not show any potassium enrichment and therefore it is not clear whether an interaction has taken place or not. If an interaction has taken place, then it is on a scale that is not detectable with the applied SEM-EDS analysis. Even if an initial attack has happened on Ni_2Al_3 a re-passivation must have occurred and has protected the coating from a continued attack. This is in striking contrast to the case of Fe_2Al_5. Even though the Fe_2Al_5 has the highest aluminum content among the investigated coatings, it shows the poorest performance. One possibility for this can be the presence of chromium-rich phases within the Fe_2Al_5 coating (Fig. 6a and b). *Vokal* et al. [9] attribute the KCl-induced attack on aluminide phases to the presence of α-Cr and/or $Cr_{23}C_6$ at the grain boundaries of the aluminide phase. In fact, in their study they report the worst corrosion for Ni_2Al_3 on a chromium-containing nickel-base alloy (Inconel 617). A detrimental effect from chromium-containing phases is consistent with the high affinity of chromium to react with alkali chlorides and form alkali chromates [39–45]. However, in the present study and under the present conditions no indications of chromium involvement were found. Rather, aluminum was often associated with potassium. Another possibility could be segregation of chromium into the grain boundaries of Fe_2Al_5 slowing down the outward diffusion of aluminum through the grain boundaries. Further investigation is necessary to assess the role of chromium-rich phases within the aluminide coatings.

5 Conclusions

Pack cementation aluminizing was employed to synthesize $Fe_{1-x}Al$ and Fe_2Al_5 diffusion coatings on the ferritic–martensitic steel P91 and a Ni_2Al_3 diffusion coating on pure Ni. The following conclusions can be drawn from what has been performed in this study:

1. All coatings showed excellent performance against air-oxidation at 600 °C.
2. $Fe_{1-x}Al$ on P91 formed a protective oxide on large parts of the surface when exposed to KCl in air. Local failures were observed, which were always associated with dilution of aluminum.
3. Fe_2Al_5 on P91 was attacked across the entire surface when KCl was present. The attack was generally in the form of selective aluminum removal. On large parts of the surface the attack did not seem to have continued. In a few cases, the coating was completely consumed and voluminous corrosion products had formed.
4. Ni_2Al_3 coated on pure Ni was passive when exposed to KCl in air.

Acknowledgments: This work was performed within the framework of the projects GREEN and MacPlus. Danish Council for Strategic Research (for grant 10093956) and European Commission (for grant 249809) are appreciated for their financial support. *John C. Troelsen*, *Flemming B. Grumsen*, and *Peter J.S. Westermann* are acknowledged for their help and technical support during this work.

6 References

[1] M. Montgomery, S. A. Jensen, U. Borg, O. Biede, T. Vilhelmsen, *Mater. Corros.* **2011**, *62*, 593.
[2] M. Montgomery, A. Karlsson, *Mater. Corros.* **1999**, *50*, 579.
[3] M. Montgomery, A. Karlsson, O. H. Larsen, *Mater. Corros.* **2002**, *53*, 121.
[4] P. Henderson, C. Davis, M. Montgomery, *VGB Powertech* **2005**, *6*, 53.
[5] M. Montgomery, O. Biede, O. H. Larsen, *Mater. Sci. Forum* **2006**, 523.
[6] M. Montgomery, S.A. Jensen, A. Hansson, O. Biede, T. Vilhelmsen, Presented at *9th Liege Conf. Mater. Adv. Power Eng.*, Liege, Belgium, **2010**, 1096.
[7] Y. S. Li, M. Spiegel, *Oxid. Met.* **2004**, *61*, 303.
[8] Y. S. Li, M. Spiegel, S. Shimada, *Mater. Chem. Phys.* **2005**, *93*, 217.
[9] V. Vokál, V. Rohr, M. J. Pomeroy, M. Schütze, *Mater. Corros.* **2008**, *59*, 374.
[10] T. J. Pan, Y. S. Li, Q. Yang, R. F. Feng, A. Hirose, *Corros. Sci.* **2011**, *53*, 2115.

[11] S. Enestam, D. Bankiewicz, J. Tuiremo, K. Mäkelä, M. Hupa, *Fuel* **2013**, *104*, 294.
[12] S. Karlsson, J. Pettersson, L. G. Johansson, J. E. Svensson, *Oxid. Met.* **2012**, *78*, 83.
[13] D. W. Mckee, D. A. Shores, K. L. Luthra, *J. Electrochem. Soc.* **1978**, *125*, 411.
[14] J. G. Smeggil, N. S. Bornstein, *J. Electrochem. Soc.* **1978**, *125*, 1283.
[15] A. Magdziarz, Z. Kalicka, *Corros. Sci.* **2007**, *49*, 1869.
[16] C. Schwalm., M. Schütze, *Mater. Corros.* **2000**, *172*, 161.
[17] J. Kalivodová, D. Baxter, M. Schütze, V. Rohr, *Mater. Corros.* **2008**, *59*, 367.
[18] G. Han, W. D. Cho, *Mater. Sci. Eng. A* **2006**, *419*, 76.
[19] G. Han, W. D. Cho, *Oxid. Met.* **2002**, *58*, 3.
[20] W. D. Cho, G. Han, *J. Mater. Eng. Perform.* **2006**, *15*, 558.
[21] J. Klöwer, *Mater. Corros.* **1996**, *47*, 685.
[22] J. Klöwer, U. Brill, U. Heubner, *Intermetallics* **1999**, *7*, 1183.
[23] H. Latreche, S. Doublet, G. Tegeder, G. Wolf, P. Masset, T. Weber, M. Schütze, *Mater. Corros.* **2008**, *59*, 573.
[24] M. C. Galetz, B. Rammer, M. Schütze, *Oxid. Met.* **2014**, *81*, 151.
[25] V. Rohr, M. Schütze, E. Fortuna, D. N. Tsipas, A. Milewska, F. J. Pérez, *Mater. Corros.* **2005**, *56*, 874.
[26] B. Rammer, T. Weber, M. Schütze, *Mater. Corros.* **2008**, *39*, 29.
[27] W. J. Cheng, Y. Y. Chang, C. J. Wang, *Surf. Coatings Technol.* **2008**, *203*, 401.
[28] L. Levin, A. Ginzburg, L. Klinger, T. Werber, A. Katsman, P. Schaaf, *Surf. Coatings Technol.* **1998**, *106*, 209.
[29] J. Metsäjoki, E. Huttunen-Saarivirta, T. Lepistö, *J. Mater. Eng. Perform.* **2010**, *20*, 298.
[30] FactSage 6.2, www.factsage.com
[31] S. Kiamehr, K. V. Dahl, M. Montgomery, M. A. J. Somers, *Mater. Corros.* **2015**, *66*, 1414.
[32] S. Kiamehr, K.V. Dahl, T. N. Lomholt, T. L. Christiansen, M.A.J. Somers, Presented at *Int. Symp. High Temp. Oxid. Corros. (ISHOC)*, Hakodate, Japan, **2014**.
[33] N. Folkeson, T. Jonsson, M. Halvarsson, L. G. Johansson, J. E. Svensson, *Mater. Corros.* **2011**, *62*, 606.
[34] J. M. Oh, M. J. McNallan, G. Y. Lai, M. F. Rothman, *Metall. Mater. Trans. A* **1986**, *17*, 1087.
[35] M. H. Rhee, M. J. McNallan, M. F. Forthman, *J. Mater. Energy Syst.* **1986**, *7*, 294.
[36] A. Zahs, M. Spiegel, H. Grabke, *Mater. Corros.* **1999**, *50*, 561.
[37] A. Zahs, M. Spiegel, H. Grabke, *Corros. Sci.* **2000**, *42*, 1093.
[38] A. W. Hassel, L. Neelakantan, A. Zelenkevych, A. Ruh, M. Spiegel, *Corros. Sci.* **2008**, *50*, 1368.
[39] Y. Shinata, Y. Nishi, *Oxid. Met.* **1986**, *26*, 201.
[40] Y. Shinata, *Oxid. Met.* **1987**, *27*, 315.
[41] Y. S. Li, M. Sanchez-Pasten, M. Spiegel, *Mater. Sci. Forum* **2004**, *461–464*, 1047.
[42] J. Lehmusto, P. Yrjas, B. J. Skrifvars, M. Hupa, *Mater. Sci. Forum* **2011**, *696*, 218.
[43] J. Lehmusto, D. Lindberg, P. Yrjas, B. J. Skrifvars, M. Hupa, *Oxid. Met.* **2011**, *77*, 129.
[44] J. Lehmusto, B. J. Skrifvars, P. Yrjas, M. Hupa, *Corros. Sci.* **2011**, *53*, 3315.
[45] J. Lehmusto, D. Lindberg, P. Yrjas, B. J. Skrifvars, M. Hupa, *Corros. Sci.* **2012**, *59*, 55.

(Received: April 27, 2016) W9047
(Accepted: July 21, 2016)

